View metadata, citation and similar papers at core.ac.uk

brought to you by CORE

東北大学機関リポジトリ TOUR Tohoku University Repository

Oxygen octahedral distortions in compressively strained SrRuO3 epitaxial thin films

著者	Daisuke Kan, Masato Anada, Yusuke Wakabayashi, Hiroo Tajiri, Yuichi Shimakawa
journal or publication title	Journal of Applied Physics
volume	123
number	23
page range	235303
year	2018-06-20
URL	http://hdl.handle.net/10097/00128259

doi: 10.1063/1.5036748

(C) 2018 Author(s).

Journal of Applied Physics

Oxygen octahedral distortions in compressively strained $SrRuO_3$ epitaxial thin films

Cite as: J. Appl. Phys. **123**, 235303 (2018); https://doi.org/10.1063/1.5036748
Submitted: 18 April 2018 . Accepted: 02 June 2018 . Published Online: 20 June 2018

Daisuke Kan, Masato Anada, Yusuke Wakabayashi, Hiroo Tajiri, and Yuichi Shimakawa

COLLECTIONS

EP This paper was selected as an Editor's Pick

ARTICLES YOU MAY BE INTERESTED IN

Synthesis science of $SrRuO_3$ and $CaRuO_3$ epitaxial films with high residual resistivity ratios
APL Materials **6**, 046101 (2018); https://doi.org/10.1063/1.5023477

Epitaxial integration and properties of $SrRuO_3$ on silicon
APL Materials **6**, 086101 (2018); https://doi.org/10.1063/1.5041940

Epitaxial strain effect in tetragonal $SrRuO_3$ thin films
Journal of Applied Physics **113**, 173912 (2013); https://doi.org/10.1063/1.4803869

Lock-in Amplifiers up to 600 MHz

© 2018 Author(s).

Oxygen octahedral distortions in compressively strained $SrRuO_3$ epitaxial thin films

Daisuke Kan,[1,a)] Masato Anada,[2] Yusuke Wakabayashi,[2] Hiroo Tajiri,[3] and Yuichi Shimakawa[1,4]

[1] *Institute for Chemical Research, Kyoto University, Uji, Kyoto 611-0011, Japan*
[2] *Division of Materials Physics, Graduate School of Engineering Science, Osaka University, Toyonaka 560-8531, Japan*
[3] *Japan Synchrotron Radiation Research Institute, SPring-8, Sayo, Hyogo 679-5198, Japan*
[4] *Integrated Research Consortium on Chemical Sciences, Uji, Kyoto 611-0011, Japan*

(Received 18 April 2018; accepted 2 June 2018; published online 20 June 2018)

We carried out the synchrotron X-ray diffraction measurements and investigated the oxygen octahedral distortions in compressively strained $SrRuO_3$ epitaxial thin films on $NdGaO_3$ substrates. We observed half-order Bragg reflections originating from the RuO_6 octahedral distortions accommodated in the compressively strained films. Our structural analysis shows that the RuO_6 octahedra are elongated along the out-of-plane direction and are rotated in the out-of-phase manner only about the out-of-plane direction. The RuO_6 rotation angle γ_{rot} is $10.9° \pm 1.2°$, which is larger than that in the bulk $SrRuO_3$. The results indicate that the substrate-induced compressive strain enhances the out-of-plane rotations while strongly suppressing the in-plane rotations. In fact, the half-order Bragg reflections arising from the octahedral rotations about the in-plane direction are found to be weak and broad, implying that the in-plane rotations exist only in the interface region, not in the entire film. This indicates that while the in-plane octahedral rotation propagates through the interfacial octahedral connections into the film, its propagation decays within the interface region because of the compressive strain. Our results indicate that both the substrate-induced strain and the interfacial octahedral connection play important roles in determining the octahedral distortions accommodated in the strained $SrRuO_3$ films. *Published by AIP Publishing.*
https://doi.org/10.1063/1.5036748

I. INTRODUCTION

A wealth of structural and physical properties of oxide heterostructures stems in part from the fact that heterostructures' lattices can accommodate a variety of oxygen coordination environments surrounding the transition metals. For perovskite oxides, whose lattice framework is formed by corner-sharing oxygen octahedra, the oxygen environments are characterized by the oxygen displacements from the ideal face-centered position and are seen as oxygen octahedral distortions, including deformations and rotations.[1–3] These distortions lead to some changes in the chemical bonds between the transition metals and oxygen and, consequently, to the changes in their orbital hybridizations, influencing the physical properties of the heterostructures. The recent investigations have revealed that the oxygen coordination environments in the oxide heterostructures are strongly influenced by the substrate-induced epitaxial strain and the interfacial octahedral connections,[4–12] highlighting the importance of evaluating the oxygen octahedral distortions accommodated in the oxide heterostructures.

The perovskite strontium ruthenate $SrRuO_3$ (SRO) is an itinerant ferromagnetic with strong uniaxial magnetic anisotropy.[13–15] The oxygen coordination environments (or the RuO_6 octahedral distortions) in the epitaxial films of this oxide have been shown to depend on epitaxial strain and interfacial structures and to affect the magnetic anisotropy.[8,16–19] Previously, it has been revealed that applying the compressive strain into SRO and introducing the RuO_6 octahedral distortions by epitaxially growing it on the orthorhombic $NdGaO_3$ (NGO) substrates stabilizes the perpendicular magnetic anisotropy.[20] A high-resolution annular bright field imaging in the scanning transmission (ABF-STEM) observations indicated the substrate-induced strain strongly suppresses the RuO_6 octahedral rotation about the $[010]_{ortho}$ direction (about the in-plane direction) in the SRO film[21] (the subscript ortho denotes the perovskite orthorhombic unit cell). However, the oxygen in the heterostructures could be three dimensionally displaced. Because extracting oxygen positions from the STEM images basically provide information on the octahedral distortions projected on only the plane normal to the observing direction, the conventional STEM-based approaches do not allow one to fully evaluate the oxygen octahedral distortions accommodated in the heterostructures. Obtaining three-dimensional oxygen positions is ideal and is important for delineating how the RuO_6 octahedral distortions affect the properties of SRO.

In this study, we carried out the synchrotron X-ray diffractions and evaluated the oxygen octahedral distortions accommodated in the compressively strained SRO films on NGO substrates. Although both bulk SRO and NGO have crystallographically the same *Pbnm* orthorhombic perovskite structure with oxygen octahedral rotations described as

[a)] E-mail: dkan@scl.kyoto-u.ac.jp

$a^-b^+a^-$ in Glazer notation, interfacial mismatches in the lattice constants and the octahedral rotation angles (or metal-oxygen-metal bond angles) would influence the RuO_6 distortions in the SRO films. We quantitatively analyzed the diffraction intensity from the SRO/NGO heterostructures, focusing on the half-order Bragg reflection intensity resulting from the distortions in the RuO_6 octahedra. We found that the substrate-induced compressive strain suppresses the in-plane RuO_6 octahedral rotations and enhances the out-of-plane ones. The RuO_6 rotations in the film can be described as $a^0a^0c^-$. Furthermore, the weak and broad reflections specifically related to the octahedral distortions in the interface region are observed. Based on the experimental observations and the quantitative analysis of the observed diffraction intensity, the oxygen octahedral distortions—including the interfacial octahedral connections—accommodated in the SRO/NGO heterostructures are discussed.

II. EXPERIMENTAL DETAILS

We employed pulsed laser deposition to epitaxially grow SRO thin films on $(110)_{ortho}$ NGO substrates. Due to the lattice mismatch between these two oxides, the substrate provides 1.7% compressive strain to the film. The SRO layer was deposited by pulsing an Ru-excess ceramic target ($SrRu_{1.3}O_x$) at 2 Hz with a KrF excimer laser (λ = 248 nm) having a laser spot density of 1.0 J/cm^2. During the deposition, the substrate temperature was kept at 700 °C, and the oxygen partial pressure was 100 mTorr. Lab-source X-ray structural characterizations, including the reciprocal space mapping measurements, confirmed the coherent growth of the films on the substrates. The film thickness was determined from the periods of thickness fringes observed in the synchrotron X-ray diffraction (00*L*) profiles.

The synchrotron X-ray diffraction measurements at room temperature were performed at the BL13XU beamline in SPring-8.[22] The details of our measurement setups were provided in our previous paper.[19] Briefly, the diffracted X-ray intensity signal observed by a PILATUS detector was corrected by the factors based on the footprint, the polarization of the incident beam, and the Lorentz factor.[23] We obtained a total of forty crystal truncation rods (CTRs) and used them to model the octahedral distortions in the SRO films (see supplementary material). The reciprocal lattice units (r.l.u.) used in this study are based on the pseudocubic perovskite lattice constants a_{pc}, b_{pc}, and c_{pc}, which are parallel to the $[1-10]_{ortho}$, $[001]_{ortho}$, and $[110]_{ortho}$ directions of the orthorhombic cell of NGO, respectively. The lattice constants a_{pc}, b_{pc}, and c_{pc} were obtained by converting the primitive cell of the orthorhombic NGO substrate (approximately $\sqrt{2}a_{pc} \times \sqrt{2}a_{pc} \times 2a_{pc}$) to the pseudocubic cell ($a_{pc} \times a_{pc} \times a_{pc}$). The lattice parameters of the nonprimitive cell of the substrate are $a_{pc} = 3.86$ Å, $b_{pc} = 3.853$ Å, $c_{pc} = 3.86$ Å ($=a_{pc}$), and $\beta_{pc} = 90.8°$.

III. RESULTS AND DISCUSSIONS

Figure 1 shows the (00L) profile for a 10-nm-thick SRO film on the NGO substrate. The (00L) Bragg reflections from both the film and the substrate are seen without any reflections originating from the secondary phases. Furthermore, the thickness fringes are obvious and persist up to L ~ 2.5, confirming high crystallinity and a sharp interface between the film and the substrate. From the positions of the (00L) Bragg reflections (L = 1 and 2), the film is found to have a larger out-of-plane lattice ($c_{pc_SRO} = 4.01$ Å) than the bulk SRO does ($c_{pc_bulkSRO} = 3.89$ Å), implying that the RuO_6 octahedra are vertically elongated by the substrate-induced compressive strain.

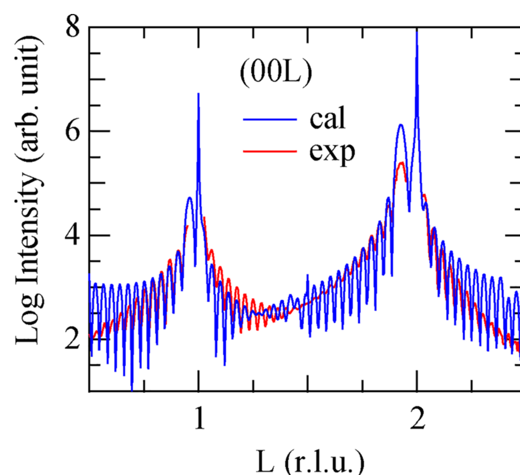

FIG. 1. Measured and calculated (00L) profiles for the 10-nm-thick SRO film on the NGO substrate. The measured and calculated profile is shown in red and blue, respectively.

To fully identify the octahedral distortions accommodated in the film, our focus is on the half-order reflections. Figure 2 shows the (1/2 1/2 L), (1/2 3/2 L), (−1 1/2 L), and (1/2 2 L) profiles for the SRO/NGO heterostructure. We found that the SRO layer exhibits a set of the half-order reflections different from those of the NGO substrate having the $a^-b^+a^-$ octahedral rotation, implying that the RuO_6 octahedral rotation pattern in the SRO layer is modified from the pattern in bulk ($a^-b^+a^-$).[24] The prominent half-order Bragg reflections from the SRO layer are seen only when H, K, and L are half-integers and H ≠ K. This behavior is

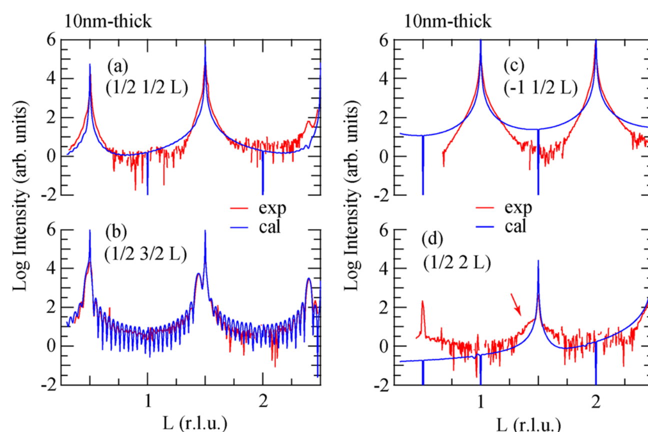

FIG. 2. Measured (red) and calculated (blue) (a) (1/2 1/2 L), (b) (1/2 3/2 L), (c) (−1 1/2 L), and (d) (1/2 2 L) profiles for the 10-nm-thick SRO film on the NGO substrate. The arrow indicates the (1/2 2 3/2) reflection from the SRO film. In (d), the peak at (1/2 2 1/2) probably originates from a minority of the crystallographic twin domain in the substrate.

TABLE I. Structural parameters for the 10-nm thick SRO film determined from the synchrotron X-ray diffraction profiles and their analysis based on the model calculations. (The details of the analysis are provided in the supplementary material.) Note that the SRO films are coherently grown on the NGO substrate and the in-plane lattice constants of SRO are fixed to be identical to those of the substrate. For SRO and NGO, the axes for a_{pc}, b_{pc} and, c_{pc} are, respectively, parallel to the $[1-10]_{ortho}$, $[001]_{ortho}$, and $[110]_{ortho}$ directions of the orthorhombic cell.

	Lattice param.	Symmetry	Rotation pattern	Rotation angle	No. of unit cells (thickness)
SRO film (on NGO sub.)	$a_{pc} = a_{NGO_pc}$ $b_{pc} = b_{NGO_pc}$ $c_{pc} = 4.0095 \pm 0.001$ Å $\beta_{pc} = 89.94 \pm 0.04°$	$I\,4/m\,c\,m$	$a^0a^0c^-$	$\alpha_{rot} = 0°$ $\beta_{rot} = 0°$ $\gamma_{rot} = 10.9° \pm 1.2°$	26 (∼104 Å)
Bulk SRO (ortho.)	$a_{pc} = 3.930$ Å $b_{pc} = 3.922$ Å $c_{pc} = 3.930$ Å $\beta_{pc} = 89.8°$	$Pbnm$	$a^-b^+a^-$	$\alpha_{rot} \sim 6.6°$ $\beta_{rot} \sim 6.2°$	
Bulk NGO (ortho.)	$a_{pc} = 3.86$ Å $b_{pc} = 3.853$ Å $c_{pc} = 3.86$ Å $\beta_{pc} = 90.8°$	$Pbnm$	$a^-b^+a^-$	$\alpha_{rot} \sim 9.3°$ $\beta_{rot} \sim 9.1°$	

confirmed for all the measured CTR profiles. Note that these half-order Bragg reflections are accompanied with clear thickness fringes whose period matches that expected from the film thickness. Our observations indicate that the out-of-phase RuO_6 octahedral rotations about the out-of-plane direction are accommodated in the SRO layer, and the rotation pattern can be described as $a^0a^0c^-$. This rotation pattern agrees well with the previous cross-sectional STEM observations for the SRO/NGO heterostructure that the octahedral rotations about the in-plane $[010]_{pc}$ direction are negligibly small.[21] Interestingly, the observed rotation pattern is identical to that in the high-temperature tetragonal phase of SRO with no A-site Sr displacements.[24] In fact, no half-order reflections related to A-site cation displacements such as (−1 1/2 1) are observed.

To quantitatively evaluate the structural parameters, we modeled the RuO_6 octahedral distortions in the film by assuming that the SRO layer has the $a^0a^0c^-$ rotations and reproduced the observed half-order Bragg reflections. The details of our structural models are provided in supplementary material. Due to the GaO_6 octahedral rotations, the NGO substrate has non-negligible contributions to the observed half-order Bragg intensity. We therefore calculated the interference between the amplitude from the SRO film and that from the substrate. The structural parameters including lattice parameters, bond lengths, and angles for the optimized structural model are summarized in Table I and supplementary material (see Fig. S2). The octahedral rotations in the SRO film are shown schematically in Fig. 3. The profiles calculated with the optimized model are also presented with the blue curves in Figs. 1 and 2. The observed CTR profiles are well reproduced with the model in which the γ rotation angle (γ_{rot}) of the RuO_6 octahedra in the SRO layer is $10.9° \pm 1.2°$. The obtained γ_{rot} value is larger than that of the bulk SRO (∼6.6°). Our analysis indicates that the substrate-induced compressive strain enhances the γ octahedral rotation while it suppresses the in-plane (α_{rot} and β_{rot}) rotations. This strain-induced octahedral behavior is consistent with the previous observations for the octahedral rotations in SRO films under negligibly small compressive strain (∼0.5%, on lattice-matched $SrTiO_3$ substrates)[25] and tensile strain (∼1%, on $GdScO_3$ substrates).[19] In contrast to the film on the NGO substrate, films on $SrTiO_3$ substrates can accommodate both out-of-plane and in-plane octahedral rotations whose magnitudes are comparable to those seen in the bulk SRO. Under the tensile strain (on $GdScO_3$ substrates), the out-of-plane (γ_{rot}) rotation was found to be suppressed while the in-plane rotation angles remain almost unchanged. The similar strain-induced changes in the oxygen octahedral rotations were also reported for $LaNiO_3$ epitaxial thin films.[4] These strain dependences on the octahedral rotations can be understood by considering that the compressive strain-induced shrinkage in the in-plane lattice favors the γ rotation, while the strain-induced elongation in the out-of-plane lattice

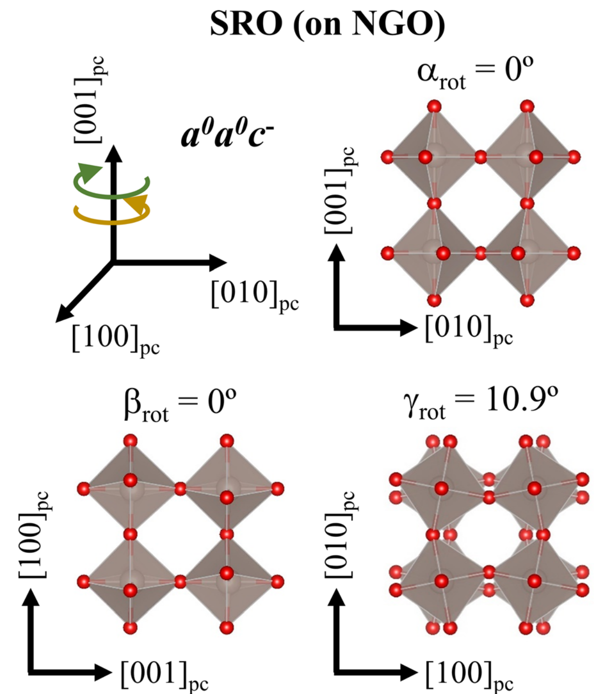

FIG. 3. Schematics of the $a^0a^0c^-$ RuO_6 octahedral rotations in the 10-nm-thick SRO film on the NGO substrate.

suppresses the octahedral rotations about the in-plane directions.

It is also worthwhile pointing out that, as indicated with the arrow in Fig. 2(d), a weak and broad (1/2 2 3/2) reflection is seen. Such a weak reflection is observed when H and L are half-integers, K is an integer, and H $\neq$ L. This indicates that the observed reflections can be attributed to the in-phase rotation about the $[010]_{pc}$ direction (the b^+ rotation). The observed profile around the (1/2 2 3/2) reflection can be reproduced by assuming that a 1.6-nm-thick (4-monolayers-thick) SRO layer has the b^+ octahedral rotations (see Fig. S3 in supplementary material). This suggests that the b^+ RuO_6 rotation exists locally in the SRO/NGO heterostructure, for example, in film/substrate interface. We also note that weak peak from the SRO layer is seen at (1/2 1/2 5/2), which can be ascribed to the out-of-phase rotation about the in-plane $[100]_{pc}$ direction (the a^- rotation). This is another implication that octahedral rotations with pattern different than that in the entire film ($a^0a^0c^-$) locally exist. We should point out that the substrate has the a^- and b^+ octahedral rotation and that the octahedral rotations in the substrate could propagate into the film region through the interfacial octahedral connection,[26] thereby stabilizing the additional RuO_6 rotation in the interface region of the film.

To further verify that the interface region of the film has the additional rotations, we investigated the half-order Bragg reflections from a 2-nm-thick SRO epitaxial film on the NGO substrate. Figure 4 shows the (1/2 1/2 L), (1/2 3/2 L), (−1 1/2 L), and (1/2 2 L) profiles. As indicated with the arrows in the profiles in the figure, the reflections from the SRO layer are obviously seen when (1) H, K, and L are half-integers, and H $\neq$ K and (2) H and L are half-integers, K is an integer, and H $\neq$ L. In addition, as suggested by slightly asymmetric profile around the (1/2 1/2 3/2) reflection, weak reflections might appear when H, K, and L are half-integers, and K $\neq$ L. The RuO_6 octahedral rotation pattern for the 2-nm-thick film can therefore be described either $a^0b^+c^-$ or $a^-b^+c^-$. Given that the substrate having the $a^-b^+a^-$ octahedral rotation is connected to the film, the latter rotation pattern is highly possible. As compared with the profiles for the 10-nm-thick film (Fig. 2), the CTR profile around the (1/2 3/2 3/2) SRO reflection, which arises from the c^- octahedral rotation, is thickness-dependent. On the other hand, the profile around the (1/2 2 3/2) SRO reflection, which originates from the b^+ rotation, is found to be almost thickness-independent. The observed behavior indicates that the entire region of the film has the c^- rotation and only the interface region has the b^+ rotation. Figure 5 schematically shows the oxygen octahedral connections across the SRO/NGO heterointerface. While the octahedral rotations propagate through the interfacial octahedral connections towards thin film region, the propagation of the octahedral rotation about the in-plane axis is strongly suppressed in the interface region. This explains the observed thickness-dependent changes in the CTR profiles of the SRO/NGO heterostructures, highlighting that the substrate-induced strain plays the important role for the accommodation of the oxygen octahedral rotations in the SRO films. We also note that the suppressed propagation of the octahedral rotation at the interface results in spatial variations of the RuO_6 rotation angles (or the Ru-O-Ru bond angles) along the out-of-plane direction. Such spatial variations of the RuO_6 rotations would significantly modulate the atomic structures in the film when the film thickness is only a couple of nanometers thick. This makes it difficult to reproduce the observed reflection intensities for the 2-nm-thick films by using the simple structural model in which the octahedral distortions including the octahedral rotation angles (the metal-oxygen bond angles) are assumed to be spatially homogeneous.

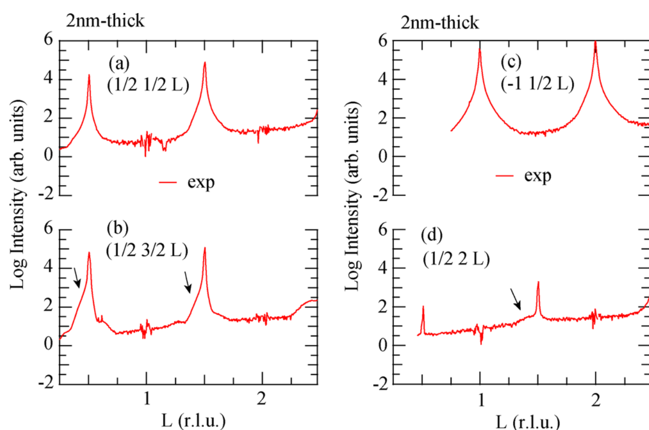

FIG. 4. (a) (1/2 1/2 L), (b) (1/2 3/2 L), (c) (−1 1/2 L), and (d) (1/2 2 L) profiles observed for the 2-nm-thick SRO film on the NGO substrate. The arrows indicate the reflections from the SRO film.

Finally, we briefly discuss the influence of the substrate-induced RuO_6 octahedral distortions on the perpendicular magnetic anisotropy in the SRO films on the NGO substrates.[20] Previously, the orbital magnetic moments, which are closely

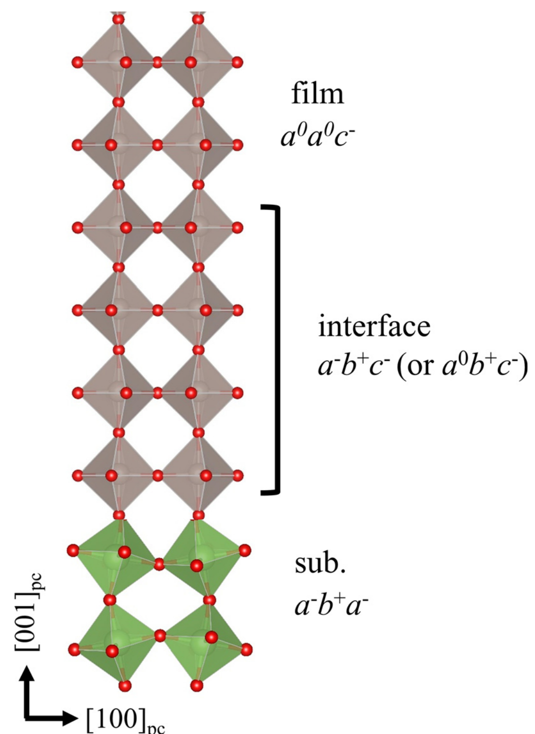

FIG. 5. Schematics of the oxygen octahedral connections across the SRO/NGO interface. The propagation of the b^+ octahedral rotation is suppressed within the interface region (∼4 monolayers thick), while the c^- rotation is accommodated in the entire SRO layer.

related to the electronic occupations of the 4d t_{2g} orbitals, are known to play a key role in determining the magnetic anisotropy of SRO films.[27,28] Our structural analysis shows that the oxygen displacements associated with the out-of-plane elongations and the c^- rotations of the RuO_6 octahedra break the degeneracy of the t_{2g} orbitals and lead to preferential occupations of d_{yz} and d_{zx} orbitals. Therefore, applying the compressive strain to SRO enhances the out-of-plane magnetic orbital moment and consequently stabilizes the perpendicular magnetic anisotropy through the spin-orbit coupling.

IV. SUMMARY

In summary, we carried out the synchrotron X-ray diffraction and quantitatively evaluated the RuO_6 octahedral distortions accommodated in the compressively strained $SrRuO_3$ epitaxial thin films grown on the $NdGaO_3$ substrates. We found that the substrate-induced strain stabilizes the out-of-plane elongation and the $a^0a^0c^-$ rotations ($\gamma_{rot} = 10.9° \pm 1.2°$) of the RuO_6 octahedra. We also observed the weak and broad reflection originating from the b^+ octahedral rotations in the interface region of the film. Our observations and structural analysis indicate that while the interfacial octahedral connection propagates the octahedral rotations, the epitaxial strain enhances the c^- rotation and suppresses the propagation of the b^+ rotation. The results highlight that both epitaxial strain and the interface structure significantly influence the octahedral distortions accommodated in the strained $SrRuO_3$ films.

SUPPLEMENTARY MATERIAL

See supplementary material for (1) details of the calculations for reflection intensities from the $SrRuO_3$ films on the $NdGaO_3$ substrates, (2) bond lengths and angles for the optimized structural model for 10 nm-thick $SrRuO_3$ film on the $NdGaO_3$ substrates, and (3) calculation of profile around the (1/2 2 3/2) reflection for the 10 nm-thick $SrRuO_3$ film on the $NdGaO_3$ substrate.

ACKNOWLEDGMENTS

This work was partially supported by a grant for the Integrated Research Consortium on Chemical Sciences and by Grants-in-Aid for Scientific Research (Grant Nos. 16H02266, 17H05217, 17H04813, and JP26105008) from the Ministry of Education, Culture, Sports, Science and Technology (MEXT) of Japan. The work was also supported by the Japan Society for the Promotion of Science (JSPS) Core-to-Core Program (A). The X-ray diffraction measurements at SPring-8 were performed with the approval of the Japan Synchrotron Radiation Research Institute (Nos. 2017A1231 and 2017B1238).

[1] A. M. Glazer, Acta Crystallogr., Sect. B **28**, 3384 (1972).
[2] A. Glazer, Acta Crystallogr., Sect. A **31**, 756 (1975).
[3] P. Woodward, Acta Crystallogr., Sect. B **53**, 44 (1997).
[4] S. J. May, J. W. Kim, J. M. Rondinelli, E. Karapetrova, N. A. Spaldin, A. Bhattacharya, and P. J. Ryan, Phys. Rev. B **82**, 014110 (2010).
[5] J. M. Rondinelli, S. J. May, and J. W. Freeland, MRS Bull. **37**, 261 (2012).
[6] Y.-M. Kim, A. Kumar, A. Hatt, A. N. Morozovska, A. Tselev, M. D. Biegalski, I. Ivanov, E. A. Eliseev, S. J. Pennycook, J. M. Rondinelli, S. V. Kalinin, and A. Y. Borisevich, Adv. Mater. **25**, 2497 (2013).
[7] E. J. Moon, R. Colby, Q. Wang, E. Karapetrova, C. M. Schlepütz, M. R. Fitzsimmons, and S. J. May, Nat. Commun. **5**, 5710 (2014).
[8] R. Aso, D. Kan, Y. Shimakawa, and H. Kurata, Adv. Funct. Mater. **24**, 5177 (2014).
[9] X. Zhai, L. Cheng, Y. Liu, C. M. Schlepütz, S. Dong, H. Li, X. Zhang, S. Chu, L. Zheng, J. Zhang, A. Zhao, H. Hong, A. Bhattacharya, J. N. Eckstein, and C. Zeng, Nat. Commun. **5**, 4283 (2014).
[10] D. Kan, R. Aso, R. Sato, M. Haruta, H. Kurata, and Y. Shimakawa, Nat. Mater. **15**, 432 (2016).
[11] Z. Liao, M. Huijben, Z. Zhong, N. Gauquelin, S. Macke, R. J. Green, S. Van Aert, J. Verbeeck, G. Van Tendeloo, K. Held, G. A. Sawatzky, G. Koster, and G. Rijnders, Nat. Mater. **15**, 425 (2016).
[12] S. S. Lee, Y. M. Kim, H. J. Lee, O. Seo, H. Y. Jeong, Q. He, A. Y. Borisevich, B. Kang, O. Kwon, S. Kang, Y. Kim, T. Y. Koo, J. S. Rhyee, D. Y. Noh, B. Cho, J. H. Seo, J. H. Lee, and J. Y. Jo, Adv. Funct. Mater. **28**, 1800839 (2018).
[13] C. B. Eom, R. J. Cava, R. M. Fleming, J. M. Phillips, R. B. vanDover, J. H. Marshall, J. W. P. Hsu, J. J. Krajewski, and W. F. Peck, Science **258**, 1766 (1992).
[14] M. Izumi, K. Nakazawa, Y. Bando, Y. Yoneda, and H. Terauchi, J. Phys. Soc. Jpn. **66**, 3893 (1997).
[15] G. Koster, L. Klein, W. Siemons, G. Rijnders, J. S. Dodge, C.-B. Eom, D. H. A. Blank, and M. R. Beasley, Rev. Mod. Phys. **84**, 253 (2012).
[16] K. Terai, T. Ohnishi, M. Lippmaa, H. Koinuma, and M. Kawasaki, Jpn. J. Appl. Phys., Part 2 **43**, L227 (2004).
[17] M. Ziese, I. Vrejoiu, and D. Hesse, Phys. Rev. B **81**, 184418 (2010).
[18] W. Lu, W. Song, P. Yang, J. Ding, G. M. Chow, and J. Chen, Sci. Rep. **5**, 10245 (2015).
[19] D. Kan, Y. Wakabayashi, H. Tajiri, and Y. Shimakawa, Phys. Rev. B **94**, 024112 (2016).
[20] D. Kan, R. Aso, H. Kurata, and Y. Shimakawa, J. Appl. Phys. **113**, 173912 (2013).
[21] R. Aso, D. Kan, Y. Fujiyoshi, Y. Shimakawa, and H. Kurata, Cryst. Growth Des. **14**, 6478 (2014).
[22] O. Sakata, Y. Furukawa, S. Goto, T. Mochizuki, T. Uruga, K. Takeshita, H. Ohashi, T. Ohata, T. Matsushita, S. Takahashi, H. Tajiri, T. Ishikawa, M. Nakamura, M. Ito, K. Sumitani, T. Takahashi, T. Shimura, A. Saito, and M. Takahasi, Surf. Rev. Lett. **10**, 543 (2003).
[23] C. M. Schleputz, R. Herger, P. R. Willmott, B. D. Patterson, O. Bunk, C. Bronnimann, B. Henrich, G. Hulsen, and E. F. Eikenberry, Acta Crystallogr., Sect. A **61**, 418 (2005).
[24] B. J. Kennedy and B. A. Hunter, Phys. Rev. B **58**, 653 (1998).
[25] R. Gao, Y. Dong, H. Xu, H. Zhou, Y. Yuan, V. Gopalan, C. Gao, D. D. Fong, Z. Chen, Z. Luo, and L. W. Martin, ACS Appl. Mater. Interfaces **8**, 14871 (2016).
[26] R. Aso, D. Kan, Y. Shimakawa, and H. Kurata, Cryst. Growth Des. **14**, 2128 (2014).
[27] K. Ishigami, K. Yoshimatsu, D. Toyota, M. Takizawa, T. Yoshida, G. Shibata, T. Harano, Y. Takahashi, T. Kadono, V. K. Verma, V. R. Singh, Y. Takeda, T. Okane, Y. Saitoh, H. Yamagami, T. Koide, M. Oshima, H. Kumigashira, and A. Fujimori, Phys. Rev. B **92**, 064402 (2015).
[28] D. Kan, M. Mizumaki, T. Nishimura, and Y. Shimakawa, Phys. Rev. B **94**, 214420 (2016).